Dalton Transactions

ROYAL SOCIETY OF CHEMISTRY

PAPER

View Article Online
View Journal | View Issue

Cite this: *Dalton Trans.*, 2025, **54**, 14040

Thermoreversible hydrogel containing photoactivatable tricarbonyl Mn(I) terpyridine complexes for therapeutic carbon monoxide (CO) release

M. Aakshika Sree and D. Amilan Jose *

Carbon monoxide (CO) is a well-established gasotransmitter known for its diverse physiological benefits. However, achieving controlled and targeted CO delivery remains challenging. To address this, light-activated carbon monoxide-releasing molecules (photoCORMs) offer a promising strategy. In this study, we report a new terpyridine-based manganese carbonyl complex, **Mn·1**, along with a known photoCORM, **Mn·2**, both capable of releasing CO upon light irradiation in various media. For the first time, these CO-releasing compounds were incorporated into the Pluronic F-127 hydrogel matrix, yielding **PG@Mn·1** and **PG@Mn·2**, respectively. Pluronic F-127 was selected due to its known biocompatibility and suitability for biomedical applications. The photo-triggered release of CO from the hydrogels was confirmed through UV-vis absorption and emission-based photokinetic studies. Additionally, time-dependent FTIR spectroscopy corroborated light-induced CO release from the hydrogel matrices. Myoglobin assays revealed that **PG@Mn·1** and **PG@Mn·2** released 3.5×10^{-2} μM and 1.71×10^{-2} μM of CO, respectively. Furthermore, **PG@Mn·1** and **PG@Mn·2** demonstrated notable antibacterial activities against *Staphylococcus aureus* and *Escherichia coli*. These findings suggest that the thermoresponsive, photoactivatable CO-releasing hydrogels **PG@Mn·1** and **PG@Mn·2** hold significant potential for future biomedical applications.

Received 29th June 2025,
Accepted 21st August 2025

DOI: 10.1039/d5dt01527h

rsc.li/dalton

Introduction

Carbon monoxide (CO) has been studied for its potential therapeutic applications for decades. Although traditionally known as a toxic gas, CO is an important endogenous gaseous signalling molecule in the human body. It exhibits several beneficial biological effects, including anti-inflammatory, antibacterial, and vasodilatory properties.[1–3] Also, CO treatment can prevent diet-induced obesity and hyperglycemia.[4] Although animal studies have demonstrated promising outcomes with CO administration, its strong affinity for hemoglobin in humans raises concerns about oxygen deprivation and related injuries. Therefore, precise delivery of CO to specific targets is essential to harness its therapeutic benefits while minimizing toxicity.[5] To address this challenge, transition metal carbonyl complexes have emerged as safe and effective carriers for CO delivery. Recently, organometallic-based Carbon Monoxide Releasing Molecules (CORMs) have gained significant attention due to their versatility and numerous advantages. These include variations in the metal center's oxidation state, structural diversity, and stereochemistry, as well as the nature and number of coordinated carbonyl ligands, all of which can be tailored to control CO release properties.[6] Notably, metal carbonyl complexes are known to release CO primarily through photodissociation upon exposure to light.[5,7,8] The chemistry of manganese carbonyl complexes is highly recommended as they are known to undergo surplus photochemical reactions.[9] Manganese (Mn), being an essential trace element, is bioessential and plays key roles in the functioning of multiple enzymes in the human body.[10] Considering the above-discussed criteria, we have reported a new manganese carbonyl complex-based CORM for the effective release of CO under light. In recent advancements, a larger number of CORMs are being reported.[2,10–12] However, water solubility is a crucial requirement for therapeutic applications, yet most CORMs lack this property. Their inherent hydrophobicity hinders efficient *in vivo* delivery, posing a significant challenge for biological use. To address this limitation, various delivery scaffolds such as polymeric micelles, lipid nanoparticles, dendrimers, and polymeric nanoparticles are employed to improve solubility and enhance bioavailability.[13,14] CO release using vesicles, liposomes, micelles, and dendrimers has been

Department of Chemistry, National Institute of Technology Kurukshetra, Kurukshetra-136119, Haryana, India. E-mail: amilanjosenit@nitkkr.ac.in

reported.[3,8,15,16] Hydrogels (HG) have received significant attention due to their vast application in the fields of biomedicine and pharmaceutics, including drug delivery, tissue engineering, and wound dressing.[17] This 3D network of hydrophilic polymer-based gels is considered a potential candidate for biomedical applications, as water is the greatest component of the human body and gels.[18,19] While biocompatibility and tunable biodegradability are advantages, their porous structure enables them to serve as a framework for incorporating the drug and protecting it from the harsh environment.[18] Stimuli-responsive hydrogels respond to physical and chemical stimuli like light, pressure, mechanical stress, pH, and various energy sources.[20,21] Temperature-responsive hydrogels are vastly favored as temperature alone serves as a trigger for gelation.[22] Thermo-reversible hydrogels undergo a sol–gel phase transition when subjected to external temperature. One of the widely used thermosensitive polymers is Pluronic, which is a Polyethylene Oxide–Polypropylene Oxide (PEO–PPO) triblock copolymer.[23] It is amphiphilic as it has hydrophobic (PPO) and hydrophilic groups (PEO).[24] Pluronic F-127 is preferred because of its ability to form a gel at lower concentrations near to room temperature (RT).[25] Due to the differing solubilities of its polyethylene oxide (PEO) and polypropylene oxide (PPO) blocks, Pluronic F-127 can self-assemble in aqueous media, and lead to the formation of micelles.[26] The micellar subunits of Pluronic act as building blocks for the gelation process. In a thermoreversible process, the micellar mode of association makes it a suitable candidate for drug delivery.[27] Although the range of application of Pluronic F-127 hydrogel is vast, its use in CO release remains unexplored. In this study, the incorporation of carboxyl- and hydroxy-functionalized Mn(I) terpyridine carbonyl complexes into a Pluronic F-127 hydrogel matrix was achieved. To the best of our knowledge, this represents the first example of such a system, providing a versatile platform for tunable, light-controlled CO delivery with potential applications in antibacterial efficiency.

Experimental section

Materials and reagents

2-Acetyl pyridine, 4-carboxybenzaldehyde, 4-hydroxybenzaldehyde, KOH, NH_4OH, diethyl ether, and Pluronic F-127 were commercially available from Sigma Aldrich. Bromopentacarbonylmanganese ($Mn(CO)_5Br$) was purchased from Alfa-Aesar. Other chemicals were purchased from Loba Chemie Pvt. Ltd. The solvents used were analytically pure and used without further purification unless otherwise specified.

Instruments and methods

Absorption and emission spectra were recorded using an Agilent Cary 60 UV-vis spectrophotometer and an Agilent Cary Eclipse fluorescence spectrometer, respectively, with a quartz cell of 1.0 cm path length. FT-IR experiments were conducted using a SHIMADZU infrared spectrophotometer. Rheological measurements were performed on a rheometer (ARES-G2). The morphology of the sample and Energy Dispersive X-ray (EDX) spectra were recorded using a JEOL JSM 6390LV SEM instrument. ^1H and ^{13}C NMR was measured on a Bruker Avance 500 MHz. The mass spectra were recorded on a Waters Q-Tof mass spectrometer.

Synthesis of 4′-(4-carboxyphenyl)-2,2′:6′,2″-terpyridine (1)

Ligand 4′-(4-carboxyphenyl)-2,2′:6′,2″-terpyridine (**1**) was synthesized following a known procedure (Fig. S1).[28] Accordingly, 2-acetyl pyridine (1.74 g, 14.38 mmol) and 4-carboxybenzaldehyde (1.08 g, 7.19 mmol) were dissolved in methanol. Later, 15% KOH and conc. NH_4OH were added to this solution. The mixture was stirred at RT for 3 days. The formed precipitate was filtered and washed with a mixture of $CHCl_3$ and cold CH_3OH/H_2O (1 : 1). The retrieved crude product was dissolved in a CH_3OH/H_2O (4 : 1) mixture. The clear solution was acidified to pH 2 using 1 M HCl, which resulted in the formation of a white precipitate. It was collected and washed with cold water to yield ligand **1**. Yield 67% (1.72 g). FTIR wavenumber (cm^{-1}): 3055, 2382, 1689, 1595, 1471, 1415, 1392, 1261, 1184, 1087, 1006, 856, 773, 729, 692, 632, 524. ESI-MS: calculated *m*/*z*: 353.11 and 354.11. Observed *m*/*z*: 354.12 and 355.12 (Fig. S2).

Synthesis of the manganese carbonyl complex (Mn·1)

$[Mn(CO)_5Br]$ (116.64 mg, 0.42 mmol) and **1** (100 mg, 0.28 mmol) were dissolved in a diethyl ether and DMF mixture, which was then refluxed for 3 hours and cooled down to RT. The resulting yellow precipitate was washed with diethyl ether to remove the unreacted $Mn(CO)_5Br$ to yield **Mn·1** as an off-white solid. Yield 62% (100 mg). FT-IR wavenumber (cm^{-1}): 2359, 2036, 1949, 1918, 1704, 1608, 1537, 1479, 1432, 1393, 1270, 1189, 1110, 1053, 1006, 858, 767, 676, and 619, where 2036, 1949, and 1918 correspond to CO stretching. ^1H NMR (500 MHz, DMSO-d_6) δ 13.26 (s, 1H), 9.33–9.20 (m, 1H), 9.08 (s, 1H), 9.02 (d, J = 8.1 Hz, 1H), 8.88–8.77 (m, 1H), 8.34–8.29 (m, 2H), 8.21 (s, 1H), 8.11 (dd, J = 22.4, 7.8 Hz, 3H), 8.05–7.89 (m, 2H), 7.70 (dt, J = 53.2, 6.4 Hz, 2H). ^{13}C NMR (126 MHz, DMSO) δ 223.85, 221.72, 217.74, 166.65, 162.96, 157.91, 157.31, 156.51, 152.97, 149.08, 148.62, 138.97, 138.83, 137.12, 132.23, 129.85, 127.86, 126.28, 124.89, 124.40, 124.26, 119.56, 35.63, 30.61. ESI-MS: calculated *m*/*z*: 572.95. Observed *m*/*z*: 569.94 and 571.94 (Fig. S3). A manganese carbonyl complex of 4′-(4-hydroxyphenyl)-2,2′:6′,2″-terpyridine (**Mn·2**) was prepared according to the previous literature reported by our group.[29]

Synthesis of Pluronic F-127 hydrogel (PG)

The Pluronic F-127 hydrogel (**PG**) was prepared by following a published procedure.[30] Out of the two techniques mentioned in the previous literature, "hot and cold techniques", we opted for the cold technique. Accordingly, 25 wt% Pluronic F-127 was slowly added to cold distilled water, along with gentle stirring. The temperature was maintained at 5 °C to dissolve the Pluronic F-127 in water until it became a clear solution. Once the Pluronic F-127 was completely dissolved, the solution was

brought to RT. The formation of **PG** was confirmed using the tube inversion method.

Incorporation of Mn·1 and Mn·2 into PG

Taking advantage of the thermoresponsive behavior, the physical state of the **PG** (solution to gel state) was tailored as needed for further studies. To achieve the homogenous distribution of **Mn·1** and **Mn·2** in the **PG**, the solution of **Mn·1** and **Mn·2** (DMSO) was added to the **PG** in its solution state (3–5 °C). Once the incorporation of **Mn·1** and **Mn·2** into the **PG** was completed, the **PG** was brought to RT. Thus, **PG** with incorporated **Mn·1** (**PG@Mn·1**) and **Mn·2** (**PG@Mn·2**) was achieved.

Photokinetic study

The CO-releasing behavior of complex **Mn·1** and gels (**PG@Mn·1** and **PG@Mn·2**) was studied using UV-vis, emission, and FTIR studies. The photolysis experiment was performed by placing the cuvette containing the CO-releasing moieties at a distance of 26 cm from the light source (410 nm, 1 W) in a covered box. It was irradiated at regular intervals until the absorption spectra showed saturation.

Myoglobin assay

A myoglobin assay was performed to quantify the CO release from **Mn·1**, **PG@Mn·1**, and **PG@Mn·2**. In this method, the conversion of deoxy-myoglobin to carbonmonoxy-myoglobin was studied spectrometrically and quantified by measuring the absorbance of the heme Q-bands at 540 nm.[31,32] Myoglobin solution (132 μM) was prepared freshly in HEPES buffer (pH 7.2). It was added to sodium dithionite (1%) to convert myoglobin into deoxymyoglobin. The CO-releasing moieties were dissolved in the deoxymyoglobin. On irradiation with the light source, the absorption band at 560 nm was converted into two absorption maxima at 540 nm and 578 nm. Later, the amount of CO released was quantified in accordance with the absorbance spectroscopy.

Time-dependent FTIR studies

Time-dependent FTIR was recorded to study the CO-releasing properties of **Mn·1**, **PG@Mn·1**, and **PG@Mn·2**. The CO-releasing moieties were irradiated systematically at regular intervals using the light source. After irradiating for a specific period, a standard amount of the sample was removed from the stock and dried to make KBr pellets. Later, the spectra were recorded for the KBr pellets.

Morphological characterization

The morphology of the hydrogels was examined using scanning electron microscopy (SEM). Prior to the analysis, the hydrogels were vacuum-dried until they became amorphous. The dried materials were spread on a double-sided conduction adhesive tape and were analyzed using SEM (JSM-6390LV, JEOL). The analysis was done under a high vacuum and at 10 kV operating voltage.

Rheological measurement

The rheological measurement of the hydrogels was performed on a rheometer (ARES-G2) along with temperature control. The parameters included a parallel plate geometry of 40 mm and a 0.2 mm gap between plates. The sol–gel transition of the hydrogels was studied by varying the temperature (5 °C min^{-1} to 10 °C min^{-1}). The viscoelastic property was studied by varying the storage (G') and loss modulus (G'').

Thermal analysis

Thermal analysis (TGA and DTA) of the hydrogels was carried out in a HITACHI TG/DTA7200. Prior to analysis, the hydrogels were vacuum-dried until they became amorphous. Later, it was placed in an aluminum pan and was heated from 30 °C to 800 °C under a N_2 atmosphere, and the changes were recorded at 10 °C min^{-1}.

Antibacterial studies

The antibacterial activities of **PG@Mn·1** and **PG@Mn·2** were studied against *Staphylococcus aureus* (*S. aureus* – MTCC 96 strain) and *Escherichia coli* (*E. coli* – MTCC 452). 0.5 McFarland standard dilution of microbes was used for the study. Ciprofloxacin (10 μg) was used as a positive control (PC). 100 μl of the diluted log cultures of bacteria was added to the microcentrifuge tube. It was added with 5 μl of the prepared treatment dilutions of **PG@Mn·1** and **PG@Mn·2** of different concentrations. After incubating for 24 hours, all the content was transferred to a 96-well plate. Once transferred, the aliquots were exposed to light irradiation (410 nm) for 1 hour. Later, the turbidity reading was recorded before and after irradiation using an ELISA Plate Reader (iMark Biorad). The minimum inhibitory concentration (MIC) value was estimated using the software GraphPad Prism-6 and using the Gompertz model.

Results and discussion

Manganese terpyridine complexes (**Mn·1** and **Mn·2**) were synthesized by refluxing their respective terpyridine ligands with $Mn(CO)_5Br$ (Scheme 1). To evaluate how substituent electronics influences CO release rates, carboxyl and hydroxyl

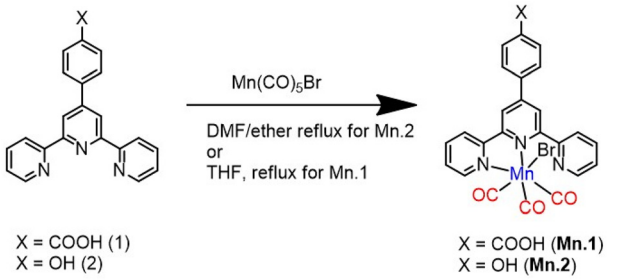

Scheme 1 Schematic representation for the synthesis of **Mn·1** and **Mn·2**.

group-substituted terpyridine complexes were selected as representative examples. The carboxyl and hydroxyl functional groups differ significantly in their electronic properties. Specifically, the carboxyl group is electron-withdrawing, while the hydroxyl group is electron-donating. All the compounds were characterized by ^{1}H NMR, ESI-MS, and FTIR analysis. Terpyridine has a wide-range of coordination chemistry, exhibiting multiple bonding modes like monodentate, bidentate, tetradentate, and bridging.[33] However, one of the familiar lower denticity bonding modes of terpyridine is bidentate.[34] Hence, we assume that **Mn·1** and **Mn·2** opt for a bidentate coordination mode, where the Mn is coordinated to the central pyridine and one terminal pyridine only, and the other terminal pyridine remains unbound.[29,34]

The FTIR spectrum of **Mn·1** exhibited two strong bands. One sharp CO stretch (ν_{CO}) was observed at 2036 cm^{-1} and another broad ν_{CO} was observed between 1949 cm^{-1} and 1918 cm^{-1}, which is in agreement with the established manganese carbonyl complexes.[35–37] A minor split was observed in this broad ν_{CO} band that distinguished the other two CO ligands present in the equatorial plane.[5]

Photokinetic studies

The new CORM **Mn·1** was subjected to a photokinetic experiment to monitor its CO-releasing behavior on exposure to light (410 nm). As shown in Fig. 1, the UV-vis spectra of **Mn·1** showed a broad absorption band at 400 nm, along with a higher-energy band at 290 nm. Upon photolysis, absorption at 400 nm decreased, with concurrent increases at 488 nm and 286 nm. The change in absorbance appeared along with clear isosbestic points at 358 nm, 313 nm, and 293 nm. This indicated the neat conversion of **Mn·1** into photolyzed products and the release of CO from the solution. The dissolution rates of acids have a broad range of solubility properties under various pH values,[38] which may affect the rate of CO release from **Mn·1**. Hence, the CO-releasing behavior of **Mn·1** was explored under light in different media and with different pH values. As presented in Table 1, the rate of CO release is faster in CH_3CN–DMSO (80–20, v/v) as compared to media with other pH conditions. The UV-vis and emission spectra obtained showed similar spectral changes in all media (Fig. 1 and 2), and CO release was slower in a neutral pH medium.

As presented in Table 1, the photochemical behaviour was compared in different media. **Mn·1** consistently has higher rate constants and shorter half-lives than **Mn·2**, indicating faster CO release kinetics. Quantum yield analysis shows a trend based on the solvent; **Mn·2** has better photochemical efficiency in organic–aqueous solvent (CH_3CN–DMSO and H_2O–DMSO) mixtures (Fig. S4) while **Mn·1** has higher quantum yields in buffered aqueous environments, particularly in borax buffer (pH 9.01). These findings reveal distinct reactivity and stability profiles for **Mn·1** and **Mn·2**, influenced by the solvent and pH environment. The presence of an electron-withdrawing group (–COOH) at **Mn·1** decreases the elec-

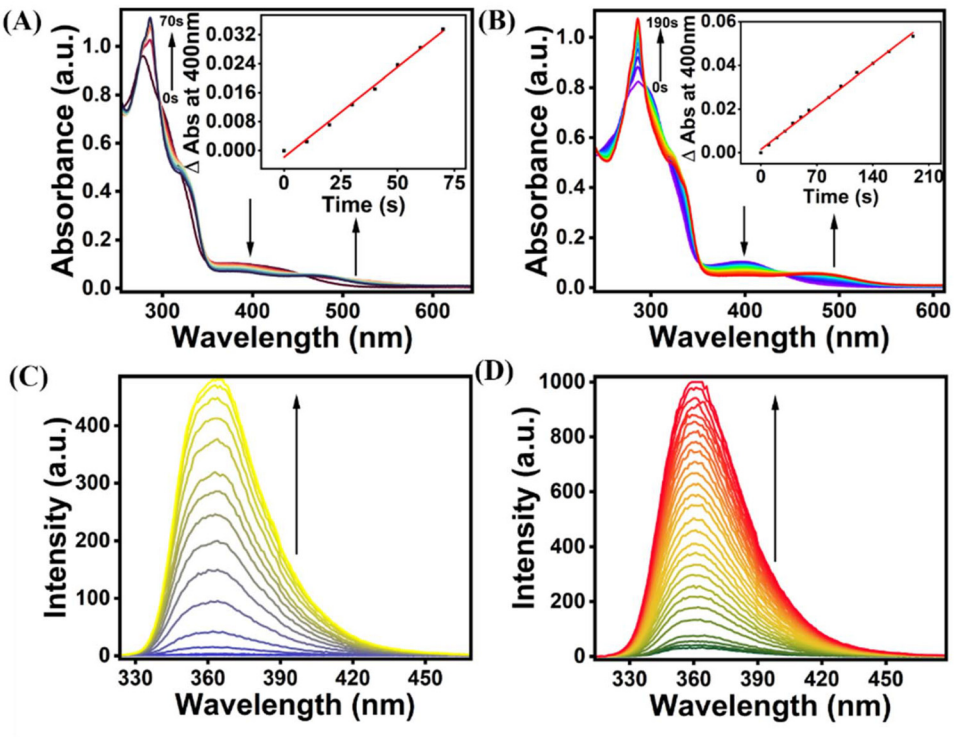

Fig. 1 Time-dependent UV-vis absorption of **Mn·1** in (A) CH_3CN–DMSO (80–20, v/v) and (B) H_2O–DMSO (80–20, v/v); emission spectra (λ_{ex} 280 nm, sw 10/10) of **Mn·1** in (C) CH_3CN–DMSO (80–20, v/v) and (D) H_2O–DMSO (80–20, v/v) upon irradiation with blue light (410 nm). Inset: the plot of change in absorbance with time.

Table 1 Comparison of the rates, $t_{1/2}$, and quantum yields of **Mn·1** and **Mn·2** in different media

	k (s^{-1})		$t_{1/2}$ (s)		Quantum yield	
Solvent media	**Mn·1**	**Mn·2**	**Mn·1**	**Mn·2**	**Mn·1**	**Mn·2**
CH_3CN–DMSO (80–20, v/v)	0.0062	0.00345	112	200	0.031931	0.067159
H_2O–DMSO (80–20, v/v)	0.00383	0.00293	181	236	0.142834	0.076379
HEPES buffer, pH = 7.2	0.00308	0.00205	225	338	0.142762	0.028636
Acetate buffer, pH = 5.01	0.00405	0.00196	171	353	0.09374	0.054591
Borax buffer, pH = 9.01	0.00432	0.00149	160	465	0.125972	0.005371

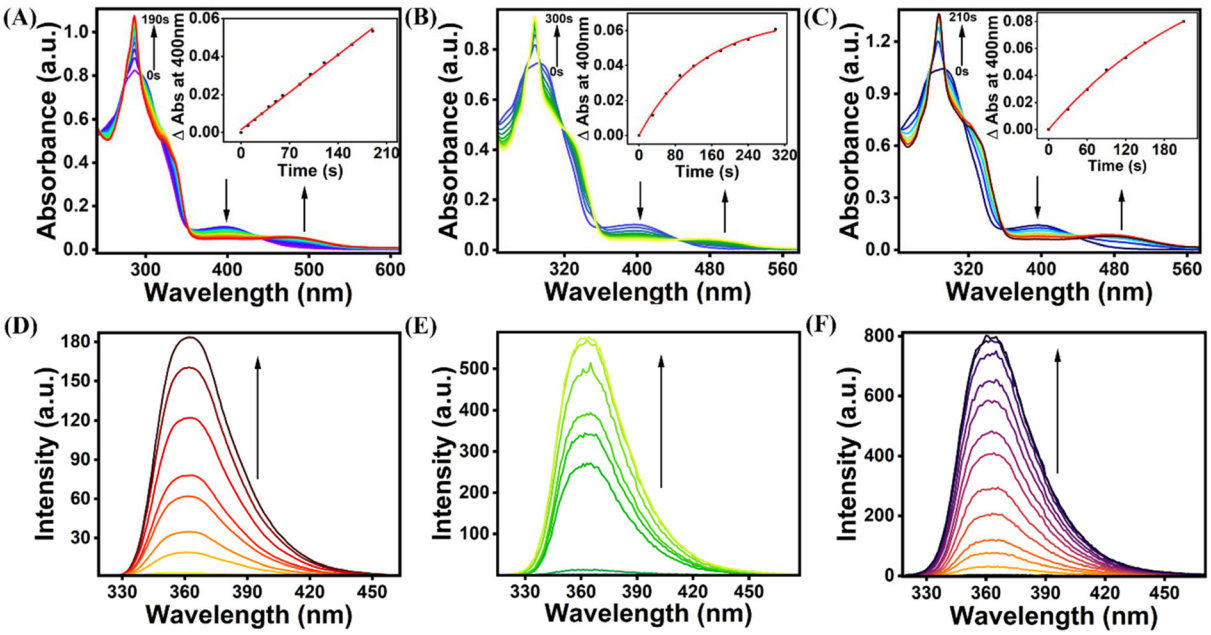

Fig. 2 Time-dependent UV-vis absorption of **Mn·1** under different pH conditions (A) HEPES buffer, pH 7.2, (B) acetate buffer, pH 5.01, (C) borax buffer, pH 9.01 and emission spectra (λ_{ex} 280 nm, sw 10/10) of **Mn·1** in (D) HEPES buffer, (E) acetate buffer, and (F) borax buffer upon irradiation with blue light (410 nm). Inset: the plot of change in absorbance with time.

tron density around the metal centre. This lowers the back bonding and may increase the CO release rate. In contrast, an electron-donating (–OH) group at **Mn·2** increases the metal density and boosts back bonding; this strengthens the metal–carbon bond and may be responsible for slow CO release as compared to **Mn·1**.[39] The rate of CO release is faster in acetonitrile for both complexes, as it quickly coordinates with Mn(I) after CO loss, preventing unstable intermediates. Also, its polar aprotic nature and fast exchange accelerate CO release, resulting in faster CO release compared to aqueous solutions.[40,41]

Furthermore, the CO-releasing behavior of **Mn·1** was also investigated using the fluorescence emission spectrum. Time-dependent emission spectra were recorded by irradiating **Mn·1** for various time periods. Initially, **Mn·1** was non-fluorescent, as the metal center is attached to the electron-withdrawing –COOH group. Upon irradiation with light, the emission intensity increased, and the complex showed strong emission at 380 nm (λ_{ex} = 280 nm). This result indicates that CO release can also be monitored by the emission OFF–ON method (Fig. 1(C), (D), and 2(D)–(F)). The increase in emission was due to the removal of CO and thereby the Mn metal from **Mn·1**, which may have led to the recovery of the terpyridine ligand (**1**) and respective emission.

Time-dependent FTIR analysis of Mn·1

Furthermore, systematic and time-dependent FTIR analysis was conducted to confirm the photo-induced release of CO from **Mn·1**. A solution of **Mn·1** in a DMSO–CH_3CN mixture was irradiated with a 410 nm light source over varying time intervals (0–1680 s). At each time point, an aliquot was withdrawn, dried under vacuum, and subsequently mixed with KBr to prepare pellets for FTIR analysis (Fig. S5(B)). As shown in Fig. S5(A), the characteristic CO stretching bands at 2022, 1950, and 1918 cm^{-1} gradually diminished with increasing irradiation time, indicating progressive CO dissociation. Notably, a visible colour change in the KBr pellets was also observed following light exposure (Fig. S5(B)), further support-

ing the complete photo release of CO from **Mn·1**. A similar change was also observed for **Mn·2** in the time-dependent FTIR studies.[29]

Myoglobin assay of Mn·1

Furthermore, the CO-releasing behavior was also confirmed using a myoglobin assay. Myoglobin solution was added with sodium dithionite (1%) to convert myoglobin into deoxymyoglobin. To this, the **Mn·1** solution (20 μM) was introduced. It was irradiated with light at various intervals, and the change in spectra was recorded. Releasing CO from **Mn·1** resulted in the conversion of deoxymyoglobin to carbonmonoxy-myoglobin, which was evident from the bands at 540 nm and 578 nm, and the isosbestic points at 552 nm and 565 nm (Fig. 3).

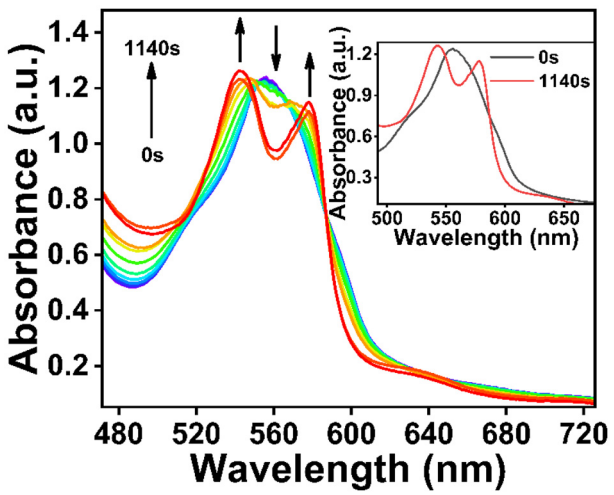

Fig. 3 UV-vis absorption spectra for the conversion of reduced Mb to Mb-CO in the solution of **Mn·1** upon exposure to light from 0 s to 1140 s. Inset: UV-vis absorption spectra of deoxy-Mb and Mb-CO.

From the myoglobin assay, it was calculated that 5.37×10^{-2} μM CO was released from 20 μM **Mn·1**, which is around 0.8 equivalents (25.6%) of CO. Following the complete release of CO from **Mn·1**, demetallation and the formation of a homoleptic Mn complex were confirmed by ESI-MS (Fig. S6). The CO-releasing behavior of **Mn·2** is already known and has been reported by us earlier.[29]

Hydrogels (HG) for CO release

Pluronic F-127 is composed of 70% poly(ethylene oxide) (PEO) units and 30% poly(propylene oxide) (PPO).[27] It has advantageous properties such as low toxicity, good drug loading capacity, and biodegradability.[42,43] In addition, Pluronic F-127 is thermosensitive, which favors cell adhesion inside the defect site.[44] Due to their enhanced site specificity, HG scaffolds have gained attention.[45] Pluronic F-127-based hydrogels (**PG**s) are known for the delivery of the gaseous signaling molecule NO.[26] But to the best of our knowledge, Pluronic F-127-based CO-releasing hydrogels are not known yet. Therefore, compounds **Mn·1** and **Mn·2** were incorporated into the Pluronic gel (**PG**) by tailoring the temperature to yield CO-releasing hydrogels **PG@Mn·1** and **PG@Mn·2**, respectively (Scheme 2). Pluronic F-127, a triblock amphiphilic copolymer, can assemble in an aqueous solution to form micelles. Pluronic F-127 solutions can undergo a sol–gel transition as temperature changes. At lower temperatures, the micelles are dispersed in the solution, resulting in a sol state. As the temperature increases, the micelles can pack together, leading to a gel-like state.[46,47]

Rheological measurement of PG@Mn·1 and PG@Mn·2

In order to obtain the desired therapeutic effect from the hydrogel, it is important to know the characteristics of its flow properties.[48] Hence, the rheological properties of both the **PG**s were studied at varying temperatures. The system composition influences the sol–gel transition process (Table 2).[27]

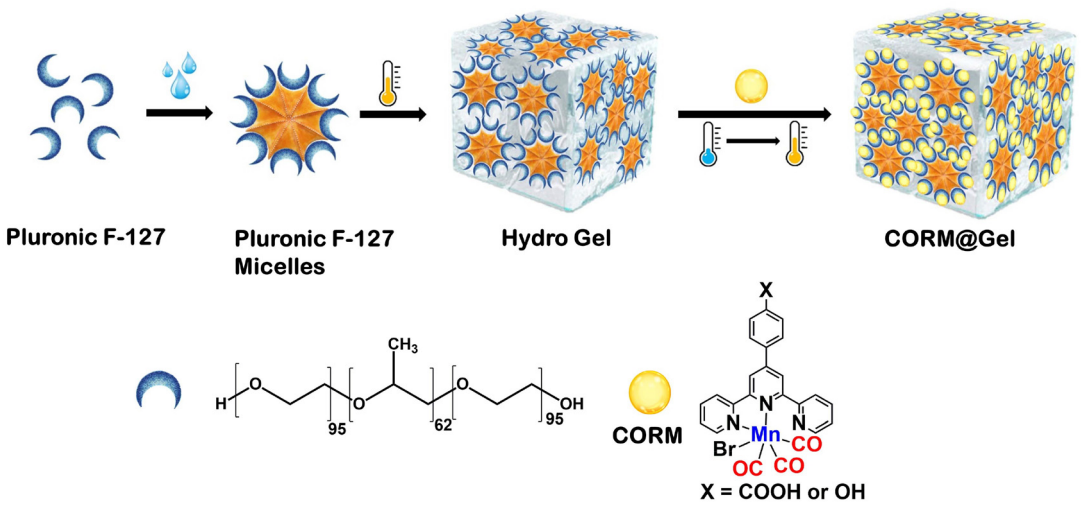

Scheme 2 Schematic representation for the incorporation of CORMs into the thermoresponsive Pluronic F-127 hydrogel (**PG**).

Table 2 Temperature range of the PGs depicting their physical state measured from rheological measurements

Hydrogel	Gel state	Sol state
Blank **PG**	20–72 °C	<20 °C and >72 °C
PG@Mn·1	~15–79 °C	<15 °C and >79 °C
PG@Mn·2	~10–82 °C	<10 °C and >82 °C

As illustrated in Fig. S7, **PG@Mn·1** and **PG@Mn·2** exhibit temperature-dependent sol–gel phase transitions. At very low and extremely high temperatures, the formulations exist in a low-viscosity sol state. In contrast, within an intermediate temperature range, they transition into a gel state. Notably, gelation occurs upon increasing the temperature above 20 °C, which can be attributed to enhanced physical entanglement among the hydrophilic PEO chains. This temperature-induced gelation behavior highlights the thermoresponsive nature of the hydrogel systems.[49] Beyond 80 °C, a gel-to-solution transition is observed, which can be attributed to dehydration of the micellar PEO shells and disruption or deformation of the gel lattice structure. This thermal behavior indicates a breakdown in the physical network stabilizing the gel, resulting in a loss of gel integrity at elevated temperatures.[50,51] Thus, rheological measurements confirm the temperature-dependent sol–gel transition behavior of the hydrogels **PG@Mn·1** and **PG@Mn·2**, highlighting their thermoresponsive nature.

Thermal analysis of PG, PG@Mn·1, and PG@Mn·2

Thermogravimetric analysis (TGA) was performed on **PG@Mn·1** and **PG@Mn·2** to evaluate their physicochemical properties and compare their thermal behavior with that of the blank **PG** (Fig. S8). The TGA curves of **PG**, **PG@Mn·1**, and **PG@Mn·2** demonstrated thermal stability up to approximately 300 °C. A rapid decomposition phase was observed between 325 °C and 420 °C, with a total weight loss of ~97%. Notably, the hydrogel formulations (**PG@Mn·1** and **PG@Mn·2**) exhibited improved thermal stability, remaining stable up to 310 °C. This indicates an extended degradation half-life compared to the individual components, suggesting that the formulation enhances the thermal stability of the hydrogel relative to the pure reactants. To investigate the heat flow characteristics, DTA was recorded for **PG**, **PG@Mn·1**, and **PG@Mn·2** (Fig. S8). The blank **PG** showed endothermic dehydration at 58 °C and exothermic decomposition at 328 °C, similar to the results in the reported literature.[52] On incorporating **Mn·1** and **Mn·2** into the **PG**, the endothermic dehydration remained at 58 °C while the exothermic dehydration slightly shifted to 291 °C for **PG@Mn·1** and 272 °C for **PG@Mn·2**, respectively. Thus, it can be concluded that even after the incorporation of **Mn·1** and **Mn·2** into the **PG**, the stability of the hydrogels is retained.

Morphological characterization of PG@Mn·1 and PG@Mn·2

Furthermore, the morphology and surface nature of **PG@Mn·1** and **PG@Mn·2** were examined by SEM and EDX analysis.

As shown in Fig. 4, **PG@Mn·1** and **PG@Mn·2** exhibited a fibrous bundle-like morphology, distinctly different from the typical structure of the blank **PG** gel. Upon incorporation of **Mn·1** and **Mn·2**, the original gel morphology was transformed into a floral-like arrangement, indicating a structural reorganization induced by the metal complexes. Elemental mapping (Fig. S9) and EDX analysis showed characteristic peaks at Kα 5.894 keV and Lα 0.637 keV, confirming the presence of manganese. These signals were observed exclusively in **PG@Mn·1** and **PG@Mn·2**, providing clear evidence of the successful incorporation of the metal complexes into the hydrogel matrix.

Furthermore, the incorporation of **Mn·1** and **Mn·2** into the **PG** was confirmed by FT-IR analysis. The spectra recorded for **PG@Mn·1** and **PG@Mn·2** displayed CO peaks analogous to those for **Mn·1** and **Mn·2**, respectively (Fig. S10).

Photokinetic study of PG@Mn·1 and PG@Mn·2

The light-induced CO-releasing ability of **PG@Mn·1** and **PG@Mn·2** was studied in both the solution and gel states by tailoring the temperature (Table 3).

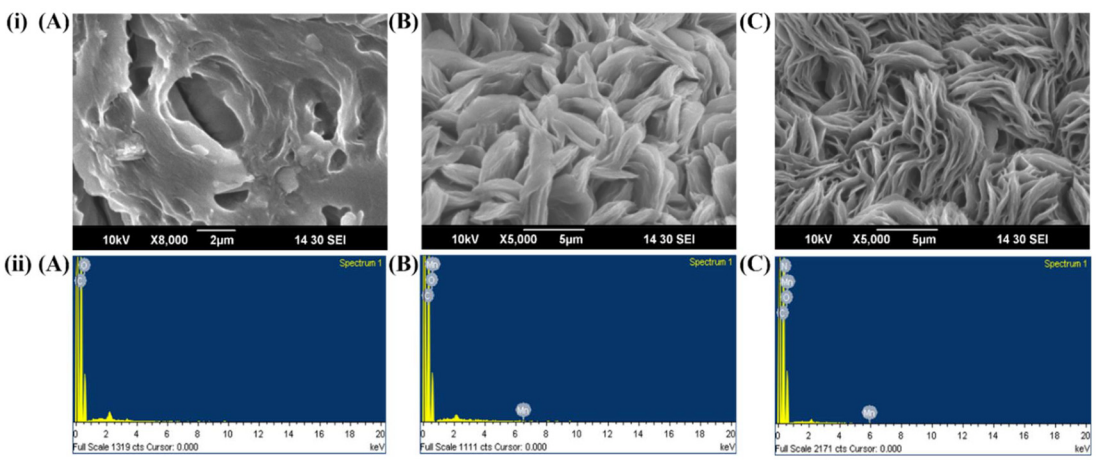

Fig. 4 (i) SEM image of (A) **PG**, (B) **PG@Mn·1**, and (C) **PG@Mn·2**. (ii) EDX of (A) **PG**, (B) **PG@Mn·1**, and (C) **PG@Mn·2**.

Table 3 Comparing the rates, $t_{1/2}$, and quantum yield of **PG@Mn·1** and **PG@Mn·2** in different physical states

Physical state	Complex	Concentration (μM)	k (s^{-1})	$t_{1/2}$ (s)	Quantum yield
Gel	**PG@Mn·1**	264.7	0.0009	796	0.050795
	PG@Mn·2	278.36	0.0074	93.77	0.344578
Liquid	**PG@Mn·1**	264.7	0.0019	359.06	0.189869
	PG@Mn·2	278.36	0.0042	165	0.263821

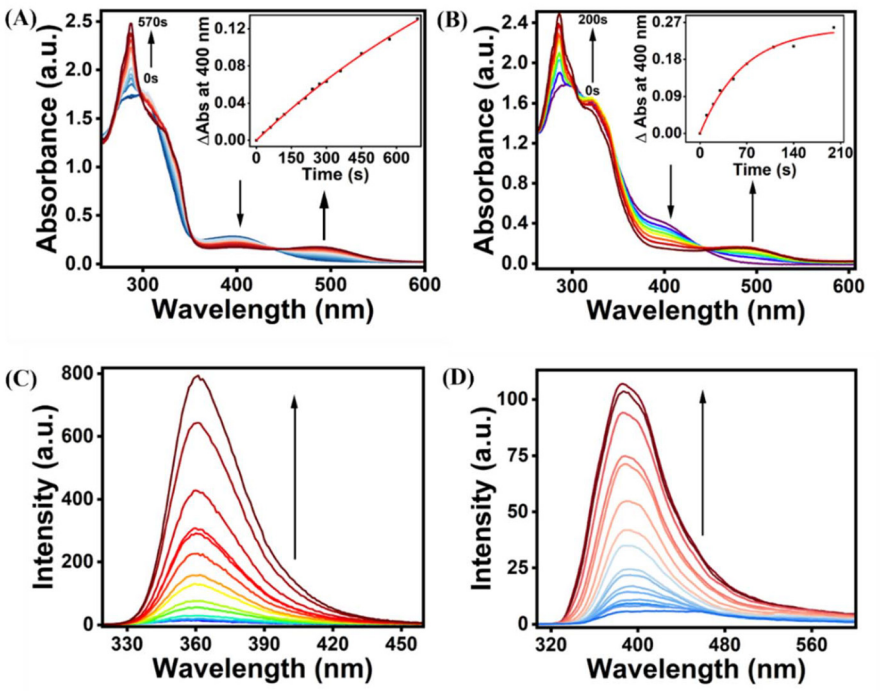

Fig. 5 Time-dependent UV-vis absorption of (A) **PG@Mn·1** and (B) **PG@Mn·2**; emission spectra (λ_{ex} 280 nm, sw 10/10) of (C) **PG@Mn·1** and (D) **PG@Mn·2** in the gel state upon irradiation with blue light (410 nm). Inset: the plot of change in absorbance with time.

The UV-vis spectra of **PG@Mn·1** in both the gel state (Fig. 5A) and the liquid state (Fig. S11(A)) show the absorption band at around 395 nm, but upon time-dependent light irradiation, an increase of the band at 488 nm and 286 nm is observed. The systematic change in the UV-vis spectrum, along with isosbestic points at 439, 353, and 294 nm, is a clear indication of CO release from both the sol and gel states of **PG@Mn·1**. The photo kinetics of CO release were also investigated using the emission spectra. **PG@Mn·1** was also non-fluorescent, but upon irradiation with light, the fluorescence was turned on at 365 nm (Fig. 5C and S11(C)). Similarly, a photokinetic study of **PG@Mn·2** was conducted. The UV-vis spectra of **PG@Mn·2** in both gel (Fig. 5B) and liquid states (Fig. S11(B)) consisted of absorption bands at 323 nm and 400 nm corresponding to intra-ligand $\pi \rightarrow \pi^*$ transition in the ligand (**2**) and MLCT, respectively.[29] On irradiation with blue light, the absorption band at 402 nm decreased, while the bands at 286 nm and 492 nm increased with isosbestic points at 446 and 304 nm. Thus, the systematic change in the absorption spectra along with the isosbestic points observed revealed the release of CO and the formation of photolyzed products. **PG@Mn·2** was also non-fluorescent initially, but upon time-dependent light irradiation, it showed that the fluorescence was turned ON at 386 nm (Fig. 5D and S11(D)). This may be due to the loss of all three CO moieties and decomplexations, which leads to the recovery of the original emission of **Mn·1** and **Mn·2**.

Therefore, from the above-discussed photokinetic study, it can be concluded that the **PG**s incorporating **Mn·1** and **Mn·2** release CO on irradiation with blue light in both gel and liquid states. Even a lower loading concentration (28 μM) of complexes is enough to release the CO from the hydrogels (Fig. S12). In this case, **PG@Mn·1** and **PG@Mn·2** released CO at rates of 0.00362 s^{-1} and 0.00436 s^{-1}, respectively.

It is evident from Fig. 6 that both the gels **PG@Mn·1** and **PG@Mn·2** remain in the same physical state before and after irradiation. Also, the CO-release from the hydrogels can be monitored through the colorimetric change. **PG@Mn·1** and **PG@Mn·2** undergo a colour change from yellow to colorless on irradiation with blue light. Thus, the gels can be used for a wider range of biological applications.

In the gel state, the polymer network is highly crosslinked, which creates a physical barrier to the movement of CO inside, while in the liquid state, the mobility of the CO is less hindered. This causes a difference in the CO release rate in both states. In the Pluronic F-127 hydrogel (gel state), CO release from **PG@Mn·1** is slower due to strong hydrogen bonding between the –COOH groups and the hydrogel network, resulting in increased crosslinking and restricted CO mobility. In contrast, **PG@Mn·2** contains –OH groups that form weaker hydrogen bonds, leading to less crosslinking and faster CO release. Additionally, hydrogels protect CO-releasing molecules from degradation as compared to other solvent systems or liposomes, ensuring stability, prolonged lifetime, and bioavailability. The stability of **Mn·1** and **Mn·2** was increased in hydrogels compared with in solution, as confirmed by UV-vis studies.

Myoglobin assay of PG@Mn·1 and PG@Mn·2

The concentration of CO released from **PG@Mn·1** and **PG@Mn·2** was calculated using the myoglobin assay by measuring the absorbance at 540 nm. On the addition of 1% sodium dithionite, myoglobin was converted into deoxymyoglobin. 20 μM **PG@Mn·1** and **PG@Mn·2** were introduced into the solution of deoxy-myoglobin. The solution was then irradiated systematically with the light source until the peak at 552 nm shifted to 542 nm and 576 nm. The isosbestic points observed and the conversion of deoxy-myoglobin to carbonmonoxy-myoglobin proved the CO release from **PG@Mn·1** and **PG@Mn·2** (Fig. S13). It was calculated that **PG@Mn·1** released 3.5×10^{-2} μM CO from 20 μM, which is around 0.5 equivalents (16.7%). Meanwhile **PG@Mn·2** released 1.71×10^{-2} μM CO from 20 μM, which is around 0.3 equivalents (8.15%). Thus, we can conclude that the amounts of **Mn·1** and **Mn·2** to be incorporated into the **PG**s can be tailored as per the requirement for CO, as **PG@Mn·1** and **PG@Mn·2** are capable of releasing CO at any concentration.

FTIR analysis of PG@Mn·1 and PG@Mn·2

Time-dependent FTIR studies were performed for **PG@Mn·1** and **PG@Mn·2** to confirm the CO release from gels. The gels irradiated with a 410 nm light source at different intervals were dried under vacuum, and the FTIR spectrum was recorded using the KBr method.

As shown in Fig. 7, the characteristic IR bands of CO at 2024, 1933, and 1912 cm^{-1} for **PG@Mn·1** and 2024, 1930, and 1908 cm^{-1} for **PG@Mn·2** disappeared on irradiation with light. This confirms the light-induced CO release from hydrogels.

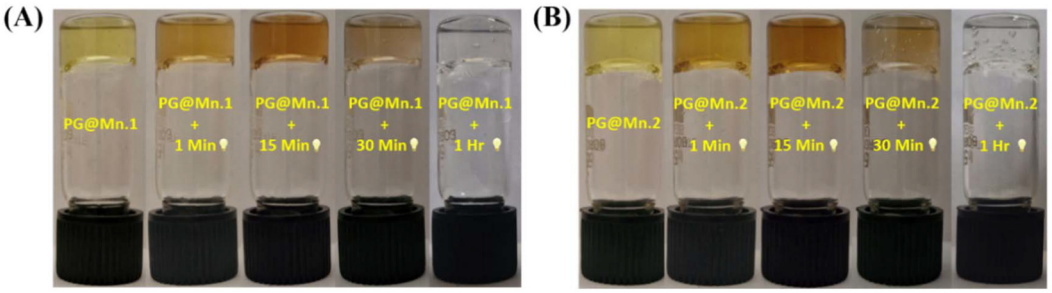

Fig. 6 Time-dependent irradiations of (A) **PG@Mn·1** (485 μM) and (B) **PG@Mn·2** (459 μM) with blue light (left to right).

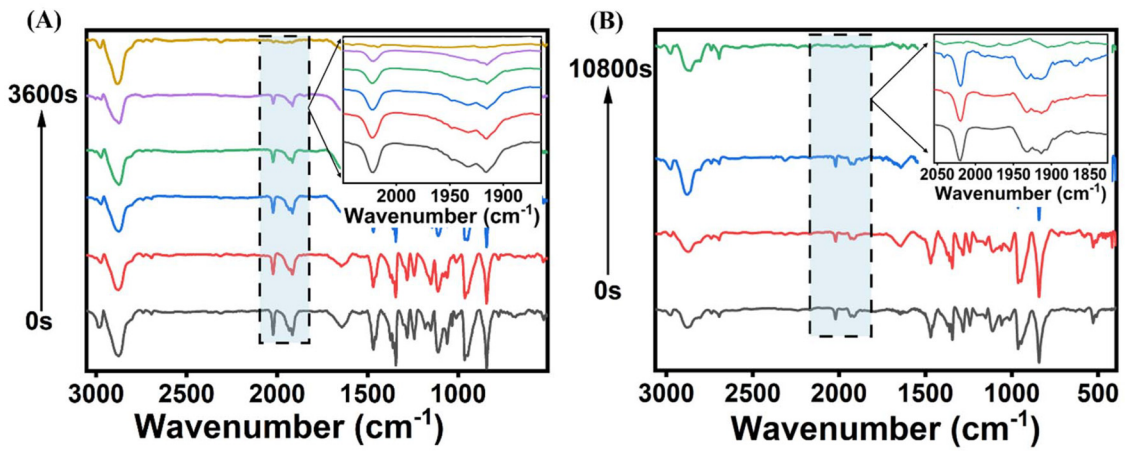

Fig. 7 Time-dependent FTIR spectrum of (A) **PG@Mn·1** and (B) **PG@Mn·2**.

Characterization of PG@Mn·1 and PG@Mn·2 after irradiation

After the release of CO from **PG@Mn·1** and **PG@Mn·2**, their physical state, morphology, and elemental distribution were examined by rheological measurements (Fig. S14), SEM analysis (Fig. 8), and elemental mapping, respectively (Fig. S15).

The hydrogels exhibited similar sol–gel–sol phase transitions before and after irradiation with blue light. Also, the

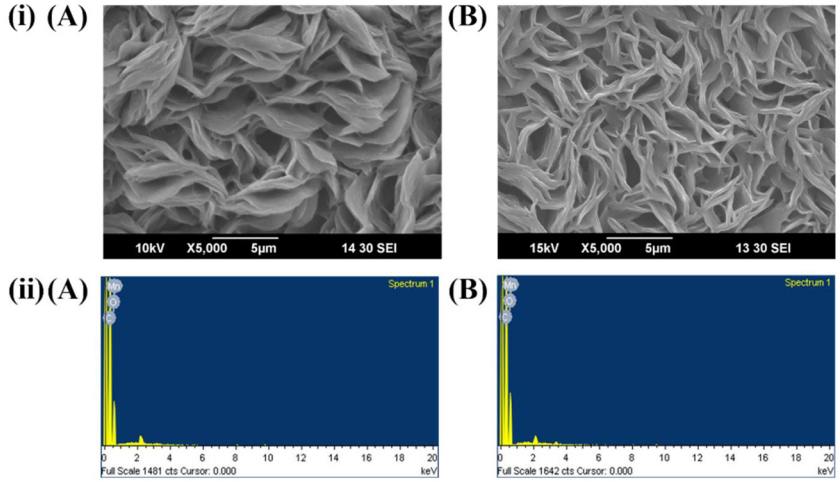

Fig. 8 (i) SEM images of (A) **PG@Mn·1** and (B) **PG@Mn·2** after irradiation. (ii) EDX of (A) **PG@Mn·1** and (B) **PG@Mn·2** after irradiation.

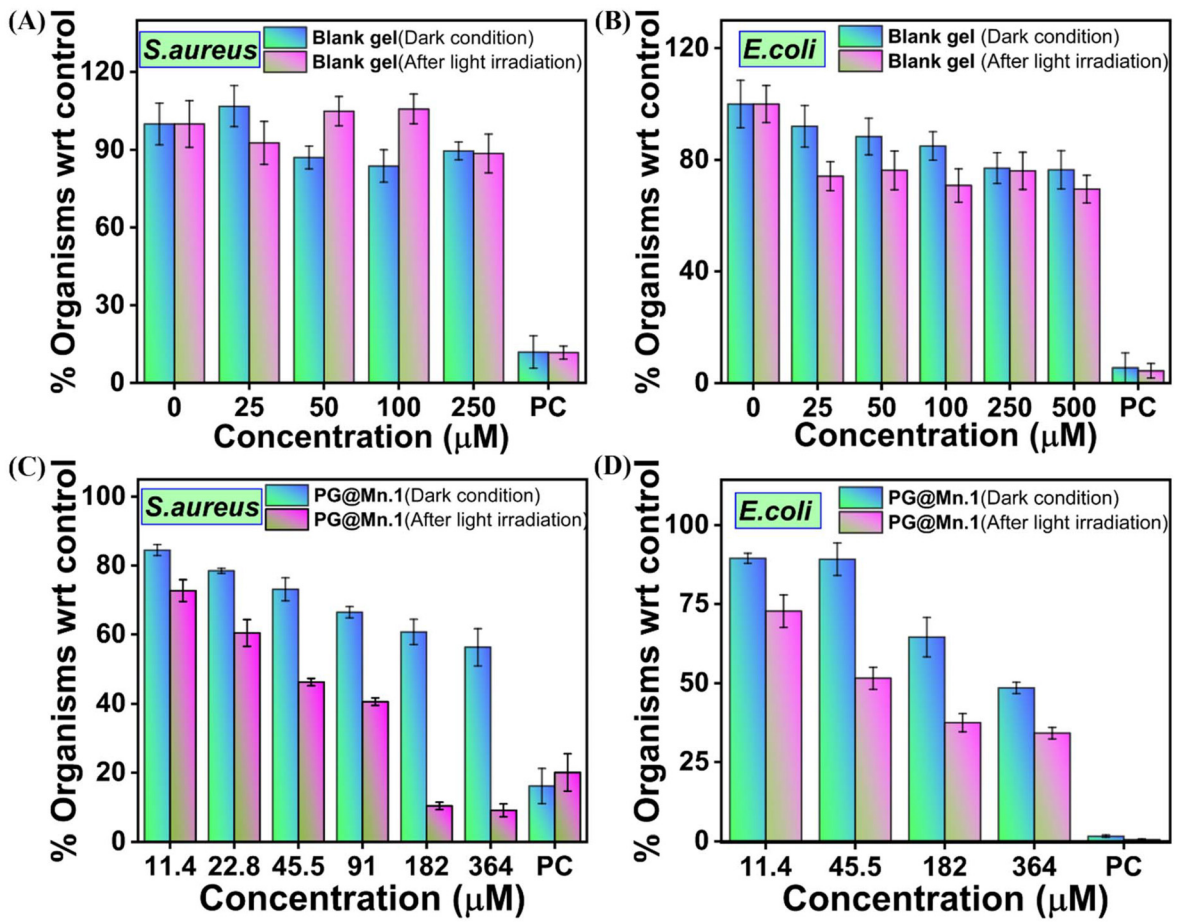

Fig. 9 MIC assay for varying concentrations of blank Pluronic F-127 gel with (A) Gram-positive (G+ve) and (B) Gram-negative (G–ve) bacteria, and for **PG@Mn·1** with (C) G+ve and (D) G–ve bacterial strains. PC denotes the positive control.

morphology of the hydrogels was similar before and after irradiation. The floral pattern of the hydrogel was retained after the irradiation, which was confirmed by SEM analysis (Fig. 8(i)).

Antibacterial activity of PG@Mn·1 and PG@Mn·2

CO is known to inhibit the growth of both Gram-positive (G+ve) and Gram-negative (G−ve) bacteria. CO-releasing molecules such as ALF021, ALF062, ALF850, ALF186, ALF153, CORM-2, CORM-3, and CORM-371 exhibited significant antibacterial properties against positive and negative bacterial strains.[53–56] Thus, the antibacterial activity of the CO-releasing hydrogel **PG@Mn·1** was explored using both G+ve (*S. aureus*) and G−ve (*E. coli*) strains. The MIC of **PG@Mn·1** was recorded before and after irradiation with blue light. As shown in Fig. 9C and D, without light irradiation, no significant effect on bacterial growth was observed with **PG@Mn·1**. But under irradiation with blue light, substantial inhibition of bacterial growth was observed. This reflects the antibacterial properties of CO released from **PG@Mn·1** on exposure to light. On the other hand, the blank gel at different concentrations exhibited no antibacterial activity, either before or after light irradiation (Fig. 9A and B). This could be because CO might potentially enhance the phagocytosis of bacteria by disrupting the bacterial cell membranes.[57] Additionally, the MIC% calculated for G+ve bacteria is 6.16% while for G−ve bacteria it is 1.32%, which signifies the potential antibacterial properties of **PG@Mn·1** with light. Similarly, **PG@Mn·2** also shows antibacterial activity against both G+ve (*S. aureus*) and G−ve (*E. coli*) strains, with the MIC% calculated for G+ve bacteria being 17.71% while that for G−ve bacteria is 12.81% (Fig. S16A and B).

Conclusion

In summary, a new CO-releasing molecule, the manganese carbonyl complex of 4′-(4-carboxyphenyl)-2,2′:6′,2″-terpyridine (**Mn·1**), was synthesized. Through a photokinetic study, the CO-releasing properties of **Mn·1** were established. **Mn·1** released 5.37×10^{-2} μM of CO on irradiation with light of 410 nm. For the first time, CO-releasing molecules **Mn·1** and **Mn·2** incorporated into thermoresponsive soft Pluronic hydrogel were prepared. The morphology and rheology of the **PG**s were studied. The morphology of the **PG** was significantly changed from a fibrous to a floral pattern on incorporation of the CORMs. The rheological experiments proved the sol–gel transition and revealed that the **PG**s stay in a liquid state at extremely low and high temperatures, while they stay in the gel state at an in-between temperature. To prove the light-induced emission of CO from **PG@Mn·1** and **PG@Mn·2**, both were subjected to a photokinetic study under light. The studies confirmed the CO-release from gels and the formation of the photolyzed products on irradiation with light. It was also observed that both **PG@Mn·1** and **PG@Mn·2** released CO in both gel and liquid states. Through the myoglobin assay, it was observed that **PG@Mn·1** and **PG@Mn·2** released 3.5×10^{-2} μM and 1.71×10^{-2} μM CO. The **PG**s remained stable under dark conditions. It was shown that both **PG@Mn·1** and **PG@Mn·2** have the ability to undergo sol–gel transition and release CO on exposure to light. In addition, the antibacterial activity of **PG@Mn·1** and **PG@Mn·2** was studied, which gave promising results. Thus, we believe that the dual advantages of **PG@Mn·1** and **PG@Mn·2** can be exploited for drug delivery applications and to facilitate easy administration.

Conflicts of interest

There are no conflicts to declare.

Data availability

The data supporting this article have been included as part of the SI: experimental details, ^{1}H-NMR and mass spectra, TG-DTA curves, rheological curves, UV and fluorescence emission kinetics spectra. See DOI: **https://doi.org/10.1039/d5dt01527h**.

Acknowledgements

DAJ gratefully acknowledges the financial support provided by the Anusandhan National Research Foundation (ANRF), New Delhi, under Core Research grant no. CRG/2022/004990; Haryana State Council for Science Innovation and Technology (HSCSIT), Haryana for Grant no. HSCSIT/R&D/2022/2949 and the Council of Scientific and Industrial Research (CSIR), India, under the CSIR-EMR(II) grant no. 01/3127/23/EMR-II. The authors also acknowledge the Central Research Facility, Indian Institute of Technology Delhi, Sonipat Campus, for providing access to rheological measurement facilities. We also thank the Department of Physics, National Institute of Technology Kurukshetra, for their assistance with the scanning electron microscopy (SEM) analysis.

References

1 L. S. Lazarus, C. T. Dederich, S. N. Anderson, A. D. Benninghoff and L. M. Berreau, *ACS Med. Chem. Lett.*, 2022, **13**, 236.
2 Y. Lai, L. Wang, H. Ma, Z. Chen, H. Wu, G. Wen, X. Wu, B. Yu, D. Li, G. Yuan, H. Huang and P. Zhang, *J. Am. Chem. Soc.*, 2025, **147**, 19353.
3 V. Kumar, Kanika, R. Khan, A. Ghosh and D. A. Jose, *Chem. – Eur. J.*, 2025, **31**, e202404062.
4 P. A. Hosick, A. A. AlAmodi, M. V. Storm, M. U. Gousset, B. E. Pruett, W. Gray, J. Stout and D. E. Stec, *Int. J. Obes.*, 2014, **38**, 132.
5 M. A. Gonzalez, M. A. Yim, S. Cheng, A. Moyes, A. J. Hobbs and P. K. Mascharak, *Inorg. Chem.*, 2012, **51**, 601.

6 S. H. Heinemann, T. Hoshi, M. Westerhausen and A. Schiller, *Chem. Commun.*, 2014, **50**, 3644.
7 R. Sakla and D. A. Jose, *Inorg. Chim. Acta*, 2021, **516**, 120134.
8 R. Sakla and D. A. Jose, *ACS Appl. Mater. Interfaces*, 2018, **10**, 14214.
9 G. J. Reiss and P. C. Kunz, *Acta Crystallogr., Sect. E: Struct. Rep. Online*, 2012, **68**, m1202.
10 A. K. Yadav, V. Singh, S. Acharjee, S. Saha, R. Kushwaha, A. Dutta, B. Koch and S. Banerjee, *Chem. – Eur. J.*, 2025, **31**, e202403454.
11 Z. Li, M. Ma, Z. Xiao, X. Jiang, X. Xu, H. Wang, P. C. Ford and X. Liu, *Appl. Organomet. Chem.*, 2025, **39**, e7959.
12 R. Sakla, A. Ghosh, V. Kumar, Kanika, P. Das, P. K. Sharma, R. Khan and D. A. Jose, *Methods*, 2023, **210**, 44.
13 A. P. Singh, A. Biswas, A. Shukla and P. Maiti, *Signal Transduction Targeted Ther.*, 2019, **4**, 33.
14 S. García-Gallego and G. J. L. Bernardes, *Angew. Chem., Int. Ed.*, 2014, **53**, 9712.
15 M. G. Hanson, R. Ambre, R. Joshi, J. D. Amidon, J. B. Snow, V. C. Lawless and B. T. Worrell, *J. Am. Chem. Soc.*, 2024, **146**, 35029.
16 P. Govender, S. Pai, U. Schatzschneider and G. S. Smith, *Inorg. Chem.*, 2013, **52**, 5470.
17 N. Nassar and S. Kasapis, *Int. J. Pharm.*, 2023, **633**, 122634.
18 Q. Chai, Y. Jiao and X. Yu, *Gels*, 2017, **3**, 6.
19 J. Nie, B. Pei, Z. Wang and Q. Hu, *Carbohydr. Polym.*, 2019, **205**, 225.
20 D. Wang and J. Hao, *Colloid Polym. Sci.*, 2013, **291**, 2935.
21 F. Ullah, M. B. H. Othman, F. Javed, Z. Ahmad and H. M. Akil, *Mater. Sci. Eng., C*, 2015, **57**, 414.
22 L. Klouda and A. G. Mikos, *Eur. J. Pharm. Biopharm.*, 2008, **68**, 34.
23 S. Liu, H. Bao and L. Li, *Eur. Polym. J.*, 2015, **71**, 423.
24 F. E. Antunes, L. Gentile, C. O. Rossi, L. Tavano and G. A. Ranieri, *Colloids Surf., B*, 2011, **87**, 42.
25 B. Shriky, A. Kelly, M. Isreb, M. Babenko, N. Mahmoudi, S. Rogers, O. Shebanova, T. Snow and T. Gough, *J. Colloid Interface Sci.*, 2020, **565**, 119.
26 H. Gzam, D. Katar, M. Tassé, Y. Xiao, I. Malfant, J. Fitremann, P. Vicendo, A.-F. Mingotaud and D. de Caro, *New J. Chem.*, 2024, **48**, 8343.
27 M. Bercea, R. Darie-Nita and S. Morariu, *Rev. Roum. Chim.*, 2013, **58**, 189.
28 A. Stublla and P. G. Potvin, *Chem. – Eur. J.*, 2010, **2010**, 3040.
29 R. Sakla, A. Singh, R. Kaushik, P. Kumar and D. A. Jose, *Inorg. Chem.*, 2019, **58**, 10761.
30 I. R. Schmolka, *J. Biomed. Mater. Res.*, 1972, **6**, 571.
31 W.-Q. Zhang, A. J. Atkin, R. J. Thatcher, A. C. Whitwood, I. J. S. Fairlamb and J. M. Lynam, *Dalton Trans.*, 2009, 4351.
32 A. J. Atkin, J. M. Lynam, B. E. Moulton, P. Sawle, R. Motterlini, N. M. Boyle, M. T. Pryce and I. J. S. Fairlamb, *Dalton Trans.*, 2011, **40**, 5755.
33 E. W. Abel, N. J. Long, K. G. Orrell, A. G. Osborne, H. M. Pain and V. Šik, *J. Chem. Soc., Chem. Commun.*, 1992, 303.
34 V. Fernández-Moreira, F. L. Thorp-Greenwood, R. J. Arthur, B. M. Kariuki, R. L. Jenkins and M. P. Coogan, *Dalton Trans.*, 2010, **39**, 7493.
35 M. S. S. Paqui, V. A. Glitz, D. C. Durigon, A. L. Amorim, G. F. Caramori, R. L. T. Parreira, A. J. Bortoluzzi, F. R. Xavier and R. A. Peralta, *Molecules*, 2023, **28**, 3439.
36 C.-C. Yang, W.-Y. Yeh, G.-H. Lee and S.-M. Peng, *J. Organomet. Chem.*, 2000, **598**, 353.
37 D. A. Kurtz, B. Dhakal, L. T. McDonald, G. S. Nichol and G. A. N. Felton, *Dalton Trans.*, 2019, **48**, 14926.
38 K. G. Mooney, M. A. Mintun, K. J. Himmelstein and V. J. Stella, *J. Pharm. Sci.*, 1981, **70**, 13.
39 U. Schatzschneider, *Br. J. Pharm.*, 2015, **172**, 1638.
40 W. C. Henke, C. J. Otolski, W. N. G. Moore, C. G. Elles and J. D. Blakemore, *Inorg. Chem.*, 2020, **59**, 2178.
41 M. Kubeil, R. R. Vernooij, C. Kubeil, B. R. Wood, B. Graham, H. Stephan and L. Spiccia, *Inorg. Chem.*, 2017, **56**, 5941.
42 S. Li, C. Yang, J. Li, C. Zhang, L. Zhu, Y. Song, Y. Guo, R. Wang, D. Gan and J. Shi, *Int. J. Nanomed.*, 2023, **18**, 4485.
43 J. C. Gilbert, J. Hadgraft, A. Bye and L. G. Brookes, *Int. J. Pharm.*, 1986, **32**, 223.
44 I. M. A. Diniz, C. Chen, X. Xu, S. Ansari, H. H. Zadeh, M. M. Marques, S. Shi and A. Moshaverinia, *J. Mater. Sci.: Mater. Med.*, 2015, **26**, 1.
45 I. Kim, W.-Y. Bang, W. H. Park, E. H. Han and E. Lee, *Nanoscale*, 2019, **11**, 17327.
46 X. Y. Xiong, K. C. Tam and L. H. Gan, *J. Nanosci. Nanotechnol.*, 2006, **6**, 2638.
47 A. Lupu, I. Rosca, V. R. Gradinaru and M. Bercea, *Polymers*, 2023, **15**, 355.
48 M. A. Malana, R. Zohra and M. S. Khan, *Korea-Aust. Rheol. J.*, 2012, **24**, 155.
49 M. J. Park and K. Char, *Macromol. Rapid Commun.*, 2002, **23**, 688.
50 C. Hopkins and J. Bruyn, *J. Rheol.*, 2019, **63**, 191.
51 M. Jalaal, G. Cottrell, N. Balmforth and B. Stoeber, *J. Rheol.*, 2017, **61**, 139.
52 E. İspir, M. Inal, Z. G. Gök and M. Yiğitoğlu, *Polym. Bull.*, 2023, **81**, 1.
53 J. Cheng and J. Hu, *ChemMedChem*, 2021, **16**, 3628.
54 L. Wareham, R. Poole and M. Tinajero-Trejo, *J. Biol. Chem.*, 2015, **290**, 18999.
55 L. S. Nobre, H. Jeremias, C. C. Romão and L. M. Saraiva, *Dalton Trans.*, 2016, **45**, 1455.
56 M. Desmard, R. Foresti, D. Morin, M. Dagouassat, A. Berdeaux, E. Denamur, S. H. Crook, B. E. Mann, D. Scapens, P. Montravers, J. Boczkowski and R. Motterlini, *Antioxid. Redox Signaling*, 2011, **16**, 153.
57 J. Chen, D. Chen, J. Chen, T. Shen, T. Jin, B. Zeng, L. Li, C. Yang, Z. Mu, H. Deng and X. Cai, *Acta Biomater.*, 2022, **146**, 49.